

X-RAY OBSERVATIONS OF THE COMA CLUSTER IN A BROAD ENERGY BAND WITH *INTEGRAL*, *RXTE* AND *ROSAT* OBSERVATORIES.

A. A. LUTOVINOV^{1,2}, A. VIKHLININ^{2,1}, E. M. CHURAZOV^{3,1}, M. G. REVNIVTSEV^{3,1}, R. A. SUNYAEV^{3,1}

Submitted to ApJ 2/24/2008

ABSTRACT

We present results of X-ray observations of the Coma cluster with multiple instruments over a broad energy band. Using the data from *INTEGRAL*, *RXTE* and *ROSAT* observatories, we find that the Coma spectrum in the 0.5–107 keV energy band can be well approximated by a thermal plasma emission model with a temperature of $T = 8.2$ keV. *INTEGRAL* was used to image the cluster emission in the hard energy band. The cluster is only marginally detectable ($\sim 1.6\sigma$) in the 44–107 keV energy band; however, the raw flux in this band is consistent with the previous results from *Beppo-SAX* and *RXTE* observatories. We can exclude with high significance that the hard-band flux reported by *Beppo-SAX* and *RXTE* could be produced by a single point source. The 20–80 keV flux of a possible non-thermal component in the cluster spectrum is $(6.0 \pm 8.8) \times 10^{-11}$ ergs cm⁻² s⁻¹. It is unlikely that the IC scattering of CMB photons is able to produce hard X-ray flux at this levels, unless the magnetic field strength is as low as 0.2 μ G. The latter value can be considered as a lower limit on the field strength in Coma. We also present a temperature map of the central part of the cluster, which shows significant variations and in particular, a hot, ~ 11.5 keV, region in the extension towards the subcluster infalling from the South-West.

Subject headings: clusters of galaxies: general — clusters of galaxies: individual(Coma)

1. INTRODUCTION

Hot intercluster medium should have an admixture of non-thermal components, including relativistic electrons, magnetic fields, relativistic protons, and supra-thermal electrons. Some of these components are expected on the theoretical grounds while the presence of relativistic electrons and sizable magnetic fields is clear from observations of cluster radio halos (see e.g. review of Ferrari et al. 2008). Often, the very existence of non-thermal components in the ICM poses interesting problems and they have been an object of intensive study (see Rephaeli et al. 2008, for a recent review). One of the important experimental probes of the relativistic electron population in clusters is the study of the high energy extension of their X-ray spectra on top of the bremsstrahlung emission of thermal plasma. This extension could be due to inverse Compton scattering of the cosmic microwave background photons (but also may arise from supra-thermal electrons (Dogiel et al. 2007)).

A classic application of the hard X-ray observation is the measurement of the bulk magnetic field strength via comparison of the inverse Compton and radio synchrotron emission (e.g. Felten & Morrison 1966, Tucker et al., 1973, Rephaeli 1979). A prime object for such studies is the Coma cluster, which possesses a bright, well-studied radio halo (see e.g. Thierbach, Klein, & Wielebinski (2003)). Since Coma is also the closest rich cluster, it was observed with virtually every X-ray observatory flown.

Detection of the hard X-ray component in excess over the extrapolation of the thermal spectrum in Coma was first reported from the *RXTE* and *Beppo-SAX* observations (Rephaeli et al. 1999; Fusco-Femiano et al. 1999), later confirmed by more extensive analyses (Rephaeli & Gruber 2002; Fusco-Femiano et al. 2004). Statistical significance of these

detections remains not very high (e.g., Fusco-Femiano et al. 2004, reported a $\sim 4.8\sigma$ detection), and are sometimes subject to criticism (e.g., an independent reanalysis of the *Beppo-SAX* data by Rossetti & Molendi 2004, leads to only a $\sim 2\sigma$ detection of the hard component). Even if a hard component exists in the Coma spectrum, we cannot exclude, on the basis of the *Beppo-SAX* or *RXTE* data, a possibility that it is produced by, e.g., a strongly absorbed AGN. Obviously, the situation can be improved through observations of Coma with and *imaging* hard X-ray telescope.

Telescopes of the *INTEGRAL* observatory (Winkler et al. 2003) offer a unique combination of good sensitivity and angular resolution in hard X-rays. The total *INTEGRAL* exposure of the Coma cluster is about 10^6 sec, leading to the sensitivity for an extended source at $E \sim 50$ keV which is comparable to that of the *Beppo-SAX* and *RXTE* data. Coma is detected by *INTEGRAL* with high significance at $E < 30$ keV, where the emission is dominated by the thermal component; the analysis in this energy band has been reported by Renaud et al. (2006) and Eckert et al. (2007). Renaud et al. (2006) used first 500 ksec of the Coma data to present first results on the Coma hard X-ray emission. The systematic analysis of a hard, non-thermal component using the full *INTEGRAL* exposure is the main emphasis of this Paper. We also present a broadband spectrum (0.5–100 keV) of Coma by combining *ROSAT*, *RXTE*, and *INTEGRAL/IBIS* data, and present a temperature map obtained from the ratio of *INTEGRAL* and *ROSAT* brightnesses.

All distance-dependent quantities are reported assuming that Coma is at $d = 90.5$ Mpc (corresponding to $z = 0.023$ and $H_0 = 70$ km s⁻¹ Mpc⁻¹).

2. OBSERVATIONS AND DATA ANALYSIS

We use X-ray observations of the Coma cluster performed by *ROSAT*, *RXTE*, and *INTEGRAL*. These observatories combined cover a very broad energy range, from 0.5 up to > 100 keV, and thus produce a very high-quality broad band spectrum. The main problem is that these instruments have

Electronic address: aal@hea.iki.rssi.ru

¹ Space Research Institute, Moscow, Russia

² Harvard-Smithsonian Center for Astrophysics, Cambridge, 02138 MA, USA

³ Max-Planck-Institut für Astrophysik, Garching, Germany

very different spatial response to the cluster emission. *ROSAT* is a direct-imaging telescope; *INTEGRAL* is a coded-mask imager which results in a rather broad Point Spread Function (PSF) in reconstructed images; *RXTE* is a collimator with a beam pattern which is slightly smaller than the cluster size. We should take these differences into account when combining the data from individual instruments. Also, the statistical quality of the Coma data in the *ROSAT* and *RXTE* energy bands is very high and so uncertainties are dominated by the instrument cross-calibration. These issues are discussed below for each telescope individually.

2.1. INTEGRAL

Coma was targeted by *INTEGRAL* in several sets of observations with a total exposure near 106 seconds (revolutions 36, 71, 72, 274, 275, 317, 318, 319, 324, 325). We concentrated here on the data from ISGRI detector (Lebrun et al. 2003) of the IBIS telescope (Ubertini et al. 2003). This telescope provides a wide field of view ($28^\circ \times 28^\circ$) and an angular resolution of $12'$. The telescope is sensitive over approximately 17–200 keV energy band. Some fraction of the IBIS data was affected by Solar flares and was discarded from the analysis. The clean set of IBIS data was initially reduced in individual pointings (so called science windows), each with a typical duration ~ 2 ksec. The reconstructed images were combined into a single mosaic which was analyzed further. The total dead-time corrected combined exposure was 990 ksec.

The IBIS/ISGRI image reconstruction algorithm was discussed previously in Krivonos et al. (2005, 2007), and we refer the reader to these works. A crucial prerequisite for this — and any other coded mask image reconstruction algorithm — is the ability to accurately predict the detector background image in the absence of any sources. Our image reconstruction software uses standard calibration tables (OSA 6.0⁴) were used to correct the event energies depending of their rise-time. We applied, however, additional corrections associated with the secular change of gain (see discussion in Tsygankov et al. 2006).

Angular size of the Coma cluster is significantly larger than the IBIS PSF. This is apparent from the comparison of the “growth function” (flux integrated within an aperture) for Coma and a point source (Crab) shown in Fig.1. While essentially all of Crab flux is concentrated within $12'$ (three $4'$ pixels in the reconstructed image), for Coma the curve continues to grow up to a $30'$ radius. In fact, the observed growth curve is consistent with that for a β -model profile, $S(r) = S_0(1 + r^2/r_c^2)^{-3\beta+0.5}$, with the parameters determined from the *ROSAT* image, $\beta = 0.741$ and $r_c = 10.7'$. Because of such a good agreement, the total Coma flux in the *INTEGRAL* energy bands can be obtained by fitting a normalization of the β -model instead of directly integrating the flux in each pixel within a wide aperture. The advantage of this method is that it provides a higher statistical accuracy since each pixel is added with an optimal weight. Direct integration, however, is less model-dependent since the hard-band thermal — and especially, the inverse Compton — emission in general does not have to follow the distribution of the surface brightness in the *ROSAT* band. Given the pros and cons, our choice is to use the β -model fluxes throughout but always check that they are consistent with the direct integration.

The limiting factor for the *INTEGRAL* observations of the

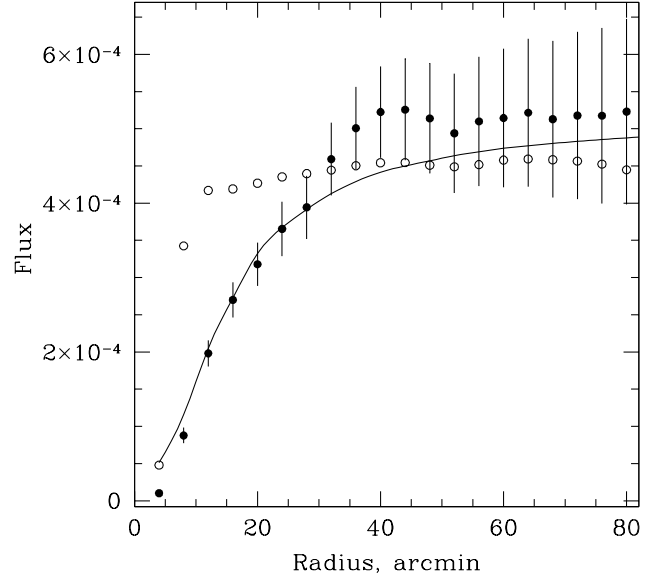


FIG. 1.— The “growth functions” (flux integrated within a given radius in the reconstructed image) of the Coma cluster (solid circles) and Crab nebula (open circles) in the 17–22 keV energy band. The solid line shows a growth curve expected for a β -model profile with $\beta = 0.741$ and $r_c = 10.7'$ (parameters for the β -model in the *ROSAT* band). The Crab flux was rescaled to the Coma level for comparison.

Coma cluster is the level of background fluctuations. In addition to purely statistical fluctuations, the background can leave systematic variations in the reconstructed image if subtracted incompletely from the raw detector image. Every care was taken, therefore, to ensure that the background was subtracted correctly. Background templates were taken from observations of “empty” fields closest in time to each Coma pointing or group of pointings. With this approach, we correctly take into account all possible temporal variations of ISGRI background. As a final check, we checked the statistics of fluctuations in the reconstructed image (similar to the analysis in §3 of Krivonos et al. (2007)), and also fluxes within $40'$ circles at different off-axis locations. In both cases, the variations had the mean consistent with zero and the dispersion equal to that expected for the purely Poisson fluctuations. We conclude, that the accuracy of our background modeling has reached its fundamental statistical limit (for the exposure time accumulated during Coma observations).

To convert ISGRI counts to physical flux units ($\text{erg s}^{-1} \text{cm}^{-2}$), we used the calibration observations of the Crab nebula which are regularly performing by *INTEGRAL*. Crab observations were reduced with the same software setup we used for Coma and the counts-to-flux conversion coefficients were determined assuming the “conventional” spectral parameters for Crab, $I = 9.7 \text{ phot s}^{-1} \text{cm}^{-2} \text{keV}^{-1}$ (Toor & Seward 1994).

After experimenting with energy bands for the Coma analysis, we chose to extract fluxes in the 17–22, 22–28.5, 28.5–44, and 44–107 keV bands. ISGRI efficiency quickly drops below 17 keV setting a natural lower limit for the energy band. The width of the two lower channels, factor of 1.3 in energy, was chosen to ensure high statistical significance of the Coma detection ($> 7\sigma$). The flux in the 44–107 keV channel should be dominated by non-thermal components. The third channel, 28.5–44 keV fills the gap.

Source fluxes were extracted within the $60'$ radius. This

⁴ <http://isdc.unige.ch>

aperture, on the one hand, contains almost all of the *INTEGRAL* X-ray flux (Fig.1), and on the other hand matches the size of the *RXTE* field of view, making flux comparisons easier. *ROSAT* pointings fully cover this region.

2.2. RXTE

Coma was observed by *RXTE* for ~ 90 ksec (Obs.ID 10368) and the data from its PCA spectrometer can be used to measure the cluster spectrum in the 3–20 keV energy band. The data reduction was done with standard programs of the LHEASOFT package (v6.0). To increase the sensitivity and reduce systematic uncertainties, we used only data of the first layers of PCA detectors. The background was based on the “L7_240CM” model (this includes both the particle-induced detector background and the all-sky average of the Cosmic X-ray Background).

One of the complications in the *RXTE* analysis is to correctly compute the flux fraction outside the PCA collimator FOV. The PCA beam pattern can be modeled as a convolution of a near-conical response of the individual collimator, $R(x, y)$, with a Gaussian ($\sigma = 6'$) which corresponds to misalignment of individual collimators and spacecraft pointing drift during the observation (Jahoda et al. 2006). $R(x, y)$ is tabulated in the calibration file *pcacol*. Assuming that in the PCA energy band, the Coma surface brightness distribution follows the *ROSAT* image, the effective flux fraction within the PCA FOV can be computed as

$$\frac{\int S(x, y) \times (R(x, y) \otimes G(x, y)) dx dy}{\int S(x, y) dx dy} = 0.763, \quad (1)$$

where $S(x, y)$ is the *ROSAT* image and $G(x, y)$ is a Gaussian. To obtain total Coma fluxes, the observed *RXTE* count rates should be divided by this factor.

In addition to the FOV correction, we need to ensure good cross-calibration of the *RXTE*/PCA with *ROSAT* and *INTEGRAL*. To this end, we note that the best-fit parameters of the Crab spectrum obtained with the standard PCA response matrix differ significantly from the “conventional” values: 2.09 ± 0.04 and 11.6 ± 0.4 phot $s^{-1} cm^{-2} keV^{-1}$ instead of 2.1 and 9.7 phot $s^{-1} cm^{-2} keV^{-1}$, respectively, indicating a possible problem with the PCA absolute calibration (Revnivtsev et al. 2003). An ad-hoc correction factor,

$$f_{corr}(E) = 0.836E^{-0.01} \quad (2)$$

applied to the observed PCA spectra brings the Crab results into agreement with the conventional average spectrum (Toor & Seward 1994). We apply this correction factor also to the Coma data. We note that this eliminates a 20% difference in flux when the PCA spectrum is extrapolated to the *ROSAT* band; the *INTEGRAL* and PCA fluxes near 20 keV are also in a good agreement after this correction is applied (Fig.2). Since we effectively base the PCA response calibration on the absolute Crab spectrum, we need to assign systematic errors to account for the uncertainties in the latter. The uncertainty of the Crab spectral index, ± 0.04 (Revnivtsev et al. 2003) can be approximated if we bin the PCA data into five wide energy channels and assign a 7% uncertainty to the flux in each channel.

2.3. ROSAT

The *ROSAT* PSPC pointed observations of Coma were reduced as described in Vikhlinin et al. (1999). The reduction pipeline was based on S. Snowden’s software (Snowden et al.

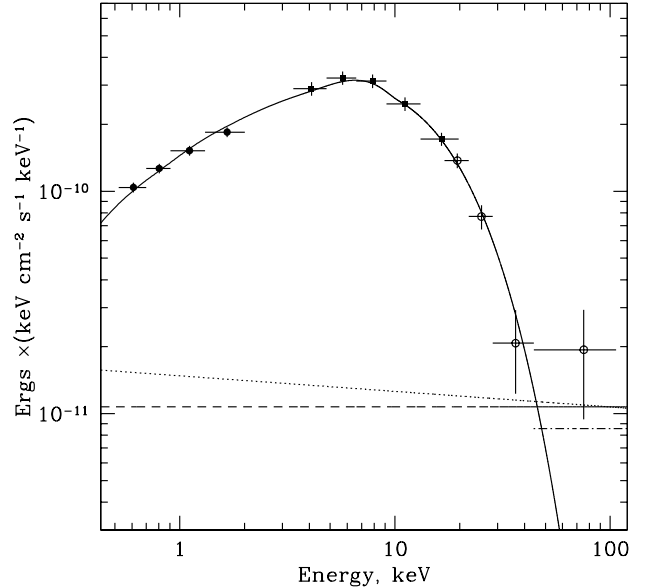


FIG. 2.— Broadband spectrum of the Coma cluster from *INTEGRAL* (open circles), *RXTE* (squares), and *ROSAT* (filled circles). The best-fit MEKAL model is shown by solid line. The contribution of non-thermal components corresponding to the Rephaeli & Gruber (2002) and Fusco-Femiano et al. (2004) detections is shown by dotted and dashed lines, respectively. A 2σ upper limit for a point source emission is shown by a dashed-dotted line.

1994). This software eliminates periods of high particle and scattered solar backgrounds as well as those intervals when the detector may be unstable. Exposure maps in several energy bands are then created using detector maps obtained during the *ROSAT* All-Sky Survey. The exposure maps include vignetting and all detector artifacts. The unvignetted particle background is estimated and subtracted from the data even though the PSPC particle background is low compared to the cosmic X-ray background. The scattered solar X-ray background also should be subtracted separately, because, depending on the viewing angle, it can introduce a constant background gradient across the image. Most of Solar X-rays were eliminated by simply excluding time intervals when this emission was high, but the remaining contribution was also modeled and subtracted. The remaining background was estimated by extracting the radial surface brightness profile from the merged data, and fitting it to the $\beta + \text{const}$ model at large radii. The background-subtracted images are suitable for direct extraction of fluxes in the energy bands of interest. Our imaging analysis uses the 0.5–2 keV band images.

3. RESULTS

3.1. Spectral analysis

The combined energy spectrum of Coma from *INTEGRAL* (17–107 keV), *RXTE* (3–20 keV), and *ROSAT* (0.5–2 keV) is shown in Fig.2. The spectrum can be well fit with the thermal plasma emission (MEKAL) with the temperature $T = 8.2 \pm 0.2$ keV, abundance fixed at 0.250 Solar (Arnaud et al. 2001), and Galactic absorption $N_H = 9 \times 10^{19} cm^{-2}$. The best-fit approximation is shown in Fig.2 by a solid line. This model gives a flux in the *INTEGRAL* band, 17–60 keV, of $f_x = 5.6 \times 10^{-11} erg cm^{-2} s^{-1}$ and luminosity $L_x = 7.1 \times 10^{43} ergs s^{-1}$. The corresponding flux and luminosity in the 2–10 keV energy band are $f_x = 4.2 \times 10^{-10} erg cm^{-2} s^{-1}$ and $L_x = 5.1 \times 10^{44} ergs s^{-1}$.

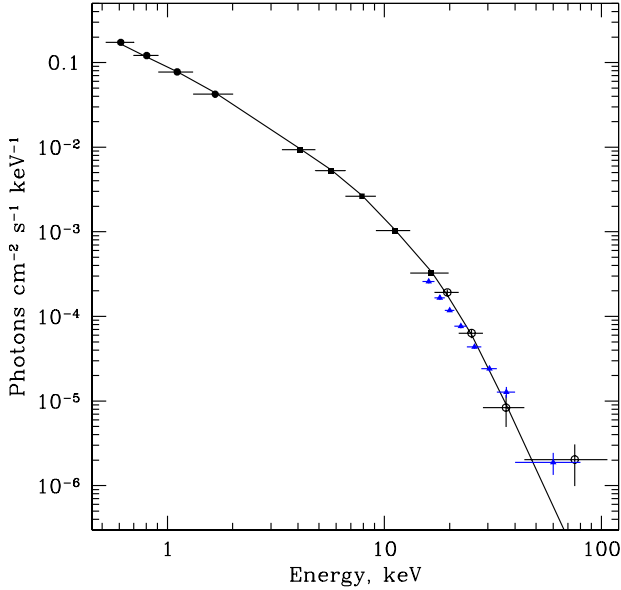


FIG. 3.— Photon spectra of Coma, derived in this work (black symbols with the same meaning as in Fig.2) and from *Beppo-SAX* (triangles, Fusco-Femiano et al. 2004). We did not adjust the normalization of the *Beppo-SAX* spectrum to account for the cluster flux outside the collimator FOV. Note the overall mismatch in spectral slope between our *RXTE* and *INTEGRAL* measurements in the 15–50 keV energy band. This has implications for the decomposition of the observed data into thermal and non-thermal components.

INTEGRAL fluxes at $E \lesssim 44$ keV are in full agreement with the thermal spectrum. The thermal component (including possible contribution from hotter regions within the cluster, see below) should make a negligible contribution at higher energies. The *INTEGRAL*-measured flux in the 44–107 keV band is $(1.8 \pm 1.1) \times 10^{-11}$ ergs cm $^{-2}$ s $^{-1}$. If real, this emission cannot be attributed to the high energy tail of the thermal spectrum and should instead represent a non-thermal component. We note, however, that the statistical significance is low (1.6σ) and *INTEGRAL* statistical uncertainties are comparable to, or higher than, those in the earlier *RXTE* or *Beppo-SAX* measurements (Rephaeli et al. 1999; Rephaeli & Gruber 2002; Fusco-Femiano et al. 1999, 2004). We also tried to repeat the Fusco-Femiano et al. (2004) procedure by fixing the photon index of a non-thermal component at $\Gamma = 2$ and fitting the total spectrum with a thermal plus power law model. This gives a power law flux of $(6.0 \pm 8.9) \times 10^{-12}$ ergs cm $^{-2}$ s $^{-1}$ in the 20–80 keV energy band (same as in Fusco-Femiano et al. 2004). This is a factor of 2.5 lower than the flux reported by Fusco-Femiano et al. (2004) in the same energy band even though we *INTEGRAL* and *Beppo-SAX* appear to measure the same flux above ~ 50 keV (Fig.3). The source of discrepancy seems to be instead in the fluxes measured at the lower boundary of the *Beppo-SAX* band. The *Beppo-SAX* data points below 20 keV seem to be a factor of 1.5–2 below our *RXTE* and *INTEGRAL* measurements, and hence they imply a lower thermal component flux. These discrepancies underscore the importance of using a broad-band spectra for detection of non-thermal components from hot clusters at around $E = 50$ keV.

Where *INTEGRAL* can do significantly better than the previous observatories is to check whether this emission can be attributed to single point source within the cluster. We do not detect any significant point sources in the hard-band im-

age (see below) and a 2σ upper limit on the point source flux is 7.6×10^{-12} ergs cm $^{-2}$ s $^{-1}$ in the 44–107 keV band. This is below the fluxes of non-thermal components reported by Fusco-Femiano et al. (2004) and Rephaeli & Gruber (2002), and so we can exclude a possibility that these detections can be attributed to a single persistent AGN.

3.2. Imaging analysis

To study the spatial structure of the cluster emission, we used images in the 17–28.5 keV (“soft”) and 44–107 keV (“hard”) *INTEGRAL* bands. The first band is a combination of two spectral channels where the cluster emission was detected with high significance; the second band is where the putative non-thermal component should dominate the thermal plasma emission. The images are shown in Fig.4. In the soft band, Coma is clearly an extended source (see Eckert et al. 2007, for detailed modeling of the *INTEGRAL* image); a point source would be confined to a $\sim 3 \times 3$ pixels square in these images.

The contours in Fig.4 show the *ROSAT* surface brightness levels in the 0.5–2 keV band. The *INTEGRAL* soft-band image shows an elongation towards the infalling subcluster and a small offset relative to the *ROSAT* surface brightness peak (see also Eckert et al. 2007). The off-set is $\sim 4.3'$ to the West (Fig.4); it is small but significant (e.g., the locations of the two AGNs detected in the Coma field, NGC 4151 and NGC 4388 are within $0.2'$ of their optical positions). As we discuss below, the offset between *INTEGRAL* and *ROSAT* images most likely reflects the temperature variations within the cluster.

We now discuss the hard-band *INTEGRAL* image (44–107 keV). As was discussed above, the total flux within $60'$ was detected in this band with a 1.6σ significance. Can this emission be associated with a small number of point sources or with an extended component centered on the cluster? The raw image (Fig.4b) does not show any significant structures. The brightest spots correspond to 1.5 – 2σ significance. In particular, we can exclude a possibility that the flux measured by *INTEGRAL* in this band can be attributed to a single point source; a 2σ upper limit is $\sim 7.6 \times 10^{-12}$ ergs cm $^{-2}$ s $^{-1}$. Figure 5 shows the hard-band image smoothed with the *ROSAT* β -model to illustrate the distribution of a more extended component. Again, there are no statistically significant features in the smoothed image. A local maximum near the Coma center is offset from the cluster location and in fact is not the brightest feature in the field. Therefore, we cannot conclude that the hard emission is spatially coincident with the Coma cluster; it is more consistent with being a statistical fluctuation.

3.3. Temperature Map

INTEGRAL’s ability to reconstruct X-ray images in the 20–30 keV band opens a unique opportunity to compute the temperature map of Coma simply from the ratio of *INTEGRAL* and *ROSAT* surface brightnesses. The *INTEGRAL* energy band is above the exponential cutoff in the thermal $T \sim 10$ keV spectrum, thus the resulting temperature map is very robust and relatively insensitive to the calibration uncertainties in either instrument.

The drawback is a relatively poor PSF of *INTEGRAL*/IBIS which results in a poor spatial resolution in the resulting temperature map. The PSF angular size is comparable to the cluster core-radius and so the *ROSAT*-to-*INTEGRAL* ratio should take into account the redistribution of flux from the center to large radii. To improve statistics, we smoothed the *INTEGRAL* image (Fig.4a) with a Gaussian with $\sigma = 5'$ that approximates the IBIS PSF in the mosaic images containing obser-

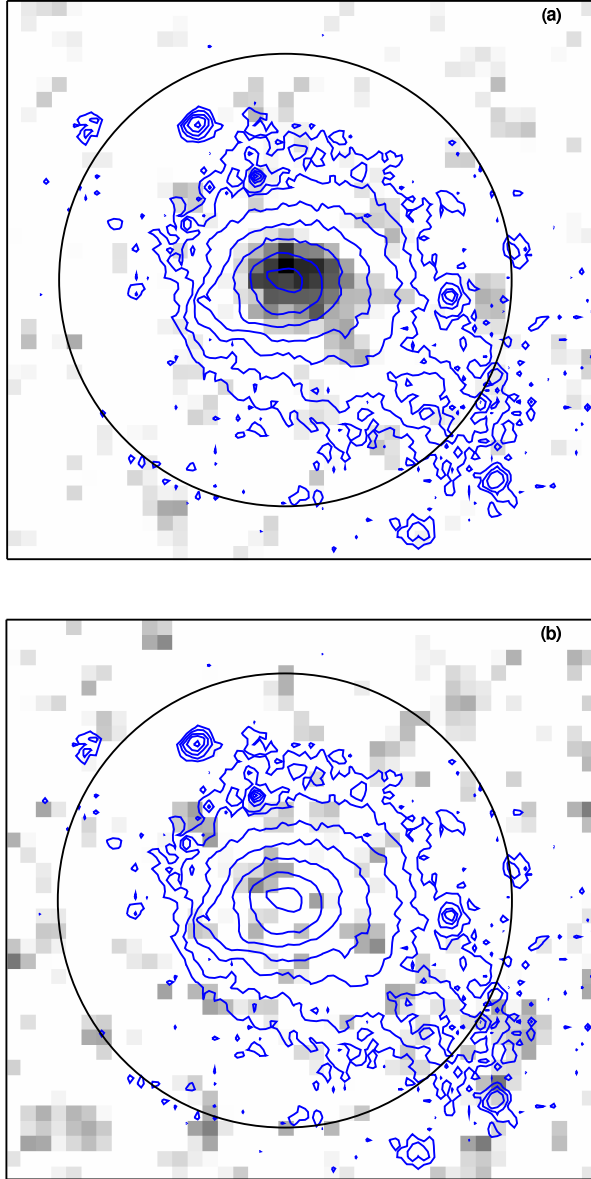


FIG. 4.— *INTEGRAL* images ($\sim 3^\circ \times 3^\circ$) of the Coma region obtained in 17–28.5 keV (a) and 44–107 keV (b) energy ranges. Contours represent the *ROSAT* intensity levels in the 0.5–2 keV energy band. Circles indicate an $r = 60'$ regions around the cluster.

variations with different rotation angles (Krivonos et al. 2007). The smoothed image has an effective PSF that can be approximated by a $\sigma = 7.1'$ Gaussian. To match the resolution of soft- and hard-band data, we smoothed the *ROSAT* image with the same Gaussian before computing the ratio map.

The obtained *INTEGRAL*-to-*ROSAT* ratio map was converted to the temperature map using a lookup table of 17–28.5 to 0.5–2 keV flux ratios for the MEKAL model as a function of temperature. As can be expected, this ratio is very sensitive to the temperature (varies by a factor of ~ 10 when T varies from 5 to 12 keV). An approximately 10σ detection of Coma by *INTEGRAL* translates into ~ 0.3 keV temperature uncertainties in the central region. The resulting temperature map is shown in Fig. 6. The map is restricted to the region where the hard X-ray flux is detected with at least 2.5σ sig-

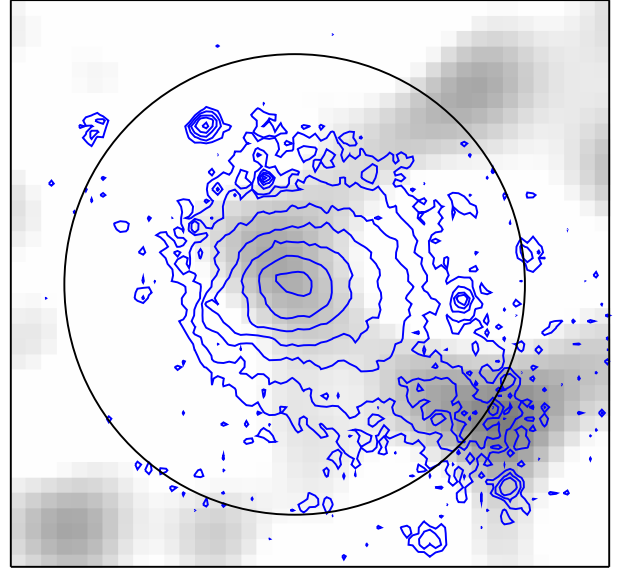


FIG. 5.— Same as in Fig. 4b, but converted with the beta-model. The gray scale is different than in Fig. 4b.

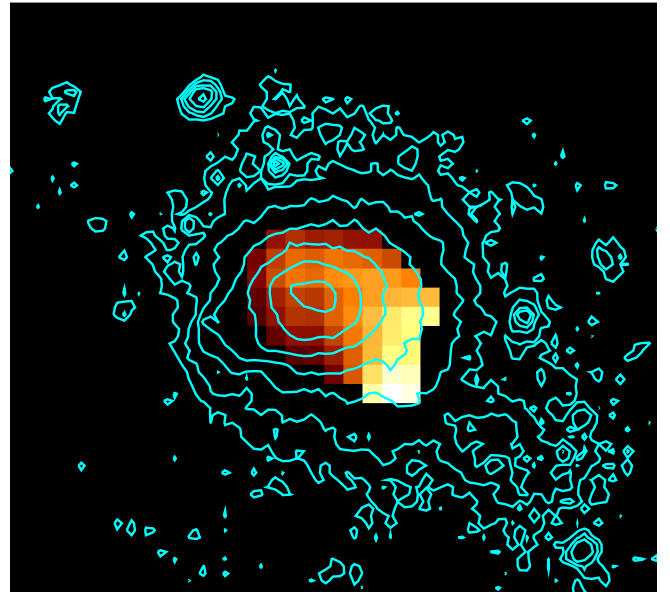


FIG. 6.— The temperature map of the central part of the Coma cluster. Temperatures of 7.5–8.5 keV, 9.5–10.5 keV and more than 11 keV correspond to brown, yellow and white colors, respectively. Contours represent the *ROSAT* intensity levels.

nificance. Qualitatively, our temperature map is similar to that obtained by Arnaud et al. (2001) from the *XMM-Newton* data. The most notable features are the cold region to the South-East of the center coinciding with a filamentary structure in the X-ray brightness (Vikhlinin et al. 1997) and the hot region in the direction of the infalling subcluster⁵.

4. DISCUSSION

⁵ This hot region was also identified by Eckert et al. (2007) with a similar technique (ratio of *INTEGRAL* and *XMM-Newton* fluxes); their temperature for this region is however higher than ours (~ 12 keV vs ~ 9.7 keV at the distance of $\sim 14'$ from the center to south-west) probably because of neglecting the *INTEGRAL* PSF effects

The possibility of using radio (synchrotron) and X-ray (Inverse Compton) observations to constrain the strength of the magnetic fields in plasma has been extensively discussed in application to various astrophysical sources (e.g. Felten & Morrison 1966, Tucker et al., 1973, Rephaeli 1979). We make similar estimates using the parameters relevant for *INTEGRAL* observations of the Coma cluster. For an electron with the Lorentz factor $\gamma \gg 1$ moving in a uniform magnetic field B at a pitch angle θ the synchrotron emission spectrum peaks at the frequency

$$\nu_r \sim 0.29 \frac{3}{4\pi} \frac{eB \sin \theta}{m_e c} \gamma^2 \quad (3)$$

(e.g., Ginzburg & Syrovatskii 1965), where m_e , e , c are the electron mass and charge, and the speed of light, respectively. The synchrotron emission of the Coma halo was observed at frequencies ranging from 30 MHz up to 1.4 GHz, and was shown to have spectral index $\alpha \sim 1.34$ (see e.g. Kim et al., 1990, Deiss et al., 1997 and references therein). At higher frequencies the evidence for spectrum steepening has been reported (Schlickeiser, Sievers & Thiemann 1987, Thierbach, Klein, & Wielebinski 2003). Below we will use the halo flux $F_r = 0.64 \pm 0.035$ Jy at $\nu_r = 1.4$ GHz reported by Deiss et al. (1997). From eq.3 it follows that emission at this frequency is provided by electrons with $\gamma_r \sim 104$ if the field is order of $10 \mu G$. We further assume that the surface brightness distribution at 1.4 GHz can also be approximated by a β -model;

$$S_r(x) \propto \left[1 + \left(\frac{x}{r_{c,r}} \right)^2 \right]^{-3\beta_r+0.5}, \quad (4)$$

where $r_{c,r}$ and β_r are the co-radius and beta-parameter of the radio surface brightness. According to Deiss et al. (1997) the scale size of the radio halo at 1.4 GHz is similar to that of the X-ray halo parameters derived by Briel, Henry & Boehringer (1992) (i.e. $r_{c,r} \sim 10''.5$, but the radio declines with radius more rapidly (i.e. $\beta_r > \beta_X = 0.75$). Colafrancesco, Marchegiani & Perola (2005) fitted the surface brightness distribution from Deiss et al. (1997) with $r_{c,r} = 23''.8$ and $\beta_r = 1.47$. The volume emissivity $\Upsilon(r)$ of the cluster (assuming spherical symmetry) at 1.4 GHz is then

$$\Upsilon_r(r) \propto \left[1 + \left(\frac{r}{r_{c,r}} \right)^2 \right]^{3\beta_r}. \quad (5)$$

We now can estimate the hard X-ray flux due to Inverse Compton scattering of CMB photons by relativistic electrons. The electron with the Lorentz factor $\gamma \gg 1$ will up-scatter CMB photons to a characteristic frequency

$$\nu_x \sim \frac{4}{3} \gamma^2 \nu_{CMB} \sim \frac{4}{3} \gamma^2 \frac{3kT_{CMB}}{h}, \quad (6)$$

where $T_{CMB} \approx 2.7K$ is the CMB temperature and k is the Boltzmann constant. Thus for the 75 keV photon the required electron Lorentz factor is $\gamma_X \sim 9 \times 10^3$, i.e. close to the value needed to produce radio emission at 1.4 GHz for plausible values of magnetic fields (see Fig.7, bottom panel). The expected IC flux due to CMB photons up-scattering produced by the electrons responsible for synchrotron emission is (Felten & Morrison 1966):

$$F_x = F_r \times C(p) \left(\frac{\nu_r}{\nu_x} \right)^\alpha T_{CMB}^{\alpha+3} B^{-\alpha-1}, \quad (7)$$

where $C(p)$ is a function of the power law slope of the electron energy spectrum, p , which is related to the synchrotron spectral index as $p = 2\alpha + 1$.

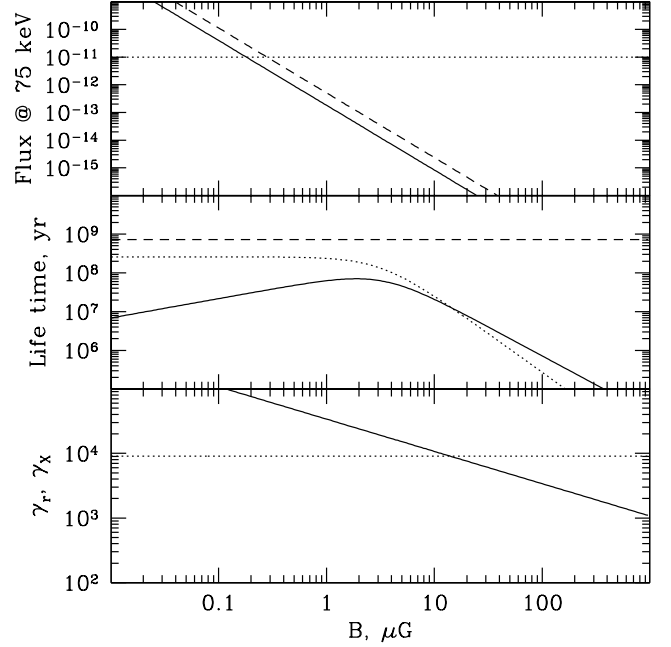


FIG. 7.— Bottom panel: Lorentz factor of electrons emitting synchrotron radiation at 1.4 GHz (γ_r , solid line) as a function of magnetic field B and the Lorentz factor of electrons producing 75 keV photons by up-scattering CMB radiation (γ_X , dotted line). Middle panel: The life time of electrons having Lorentz factors γ_r γ_X (solid and dotted lines respectively). Top panel: Sensitivity level of ISGRI/INTEGRAL at 75 keV (dotted line) in comparison with the expected level of IC emission for a given halo flux at 1.4 GHz and given uniform magnetic field B . The dashed line shows the same IC level, but scaled by a factor of 2.8 to illustrate the changes introduced by the assumption that magnetic fields energy density follows the thermal gas density distribution in cluster.

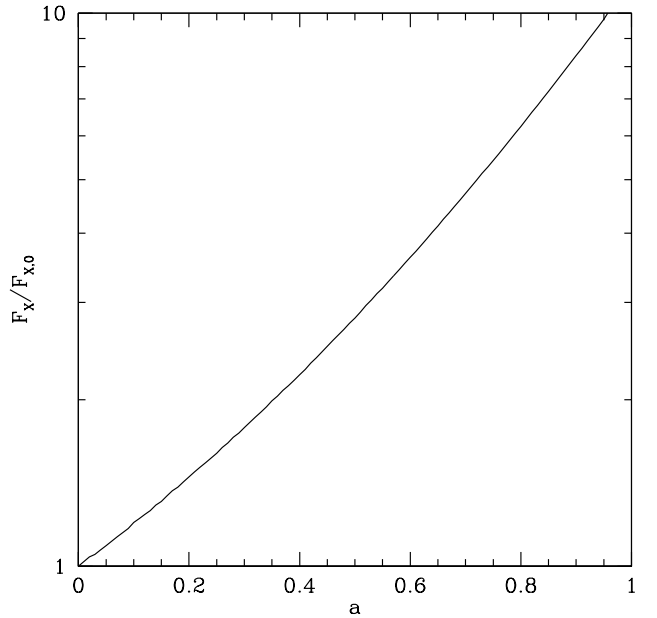


FIG. 8.— Variations of IC flux on the different behavior of the magnetic field with radius. The parametrization is done in the form $B2(r) = B2_0 \left(\frac{\rho(r)}{\rho_0} \right)^a$. See text for details.

Assuming that B is constant across the cluster, one can calculate expected IC flux for a given B and radio flux F_r using

eq.7 as is done in the top panel of Fig.7. The intersection of the predicted (solid line) and observed (dotted line) curves gives the value of the magnetic field needed to explain radio and hard X-ray fluxes as the synchrotron and IC emission respectively produced by the same electron population. The resulting $B \sim 0.2 \mu\text{G}$ is an order of magnitude smaller than the value derived from Faraday rotation $B \sim 1.7 \mu\text{G}$ (e.g., Kim et al. 1990).

The assumption of constant B across the cluster probably is too simplistic, especially given that energy density of the ICM varies strongly from the center to outskirts (see e.g. Dolag, Bartelmann & Lesch, 2002). This might affect the relation of the synchrotron and IC fluxes as discussed by Colafrancesco, Marchegiani & Perola (2005). We estimate the effects of magnetic field variations using a simple parametrization,

$$B2(r) = B2_0 \left(\frac{\rho(r)}{\rho_0} \right)^a, \quad (8)$$

where $\rho(r)$ is the thermal gas density, which scales approximately as the ICM pressure if the gas density variations are much stronger than those of temperature over the region of interest. Adopting the *ROSAT* β -model for the gas density distribution, we can write:

$$B2(r) = B2_0 \left[1 + \left(\frac{x}{r_{c,x}} \right)^2 \right]^{-\frac{3}{2}a\beta_x}, \quad (9)$$

where B_0 is the magnetic field at the center of the cluster. In this parametrization $a = 0$ corresponds to the case of a constant magnetic field, while $a = 0.5$ implies that energy density of the magnetic field scales as the ICM pressure. Compared to the constant B case (i.e. eq.7) the ratio of the IC and synchrotron fluxes (within given distance from the center) has to be multiplied by an additional factor $f(a)$:

$$f(a) = \frac{\int \Upsilon_r(r) \left(\frac{B}{B_0} \right)^{-\alpha-1} r^2 dr}{\int \Upsilon_r(r) r^2 dr}, \quad (10)$$

where $\Upsilon_r(r)$ is given by eq.5. The integration is done from zero radius up to $r_{\text{max}} = 60'$. $f(a)$ is shown in Fig.8. In these calculations we assumed $r_{c,r} = r_{c,x} = 10'.68$, $\beta_r = \beta_x = 0.741$.

The total IC flux (up to infinity) may actually diverge for large a since the drop of the B at large distances from the center has to be “compensated” by energy density of relativistic particles to maintain the assumed $\Upsilon E(r)$. This causes strong increase of IC emission. Formally for convergence (up to infinity) one needs:

$$a < \frac{2(2\beta_r - 1)}{\beta_x(\alpha + 1)}, \quad (11)$$

i.e. for our parameters, $a < 0.55$. However beta model may become poor approximation at some distance from the center which makes the outcome of the whole exercise very uncertain. From Fig.8 it follows that when fluxes are integrated over

1° circle the change in a from 0 to 0.5 changes the ratio by a factor of 2.8. Perhaps similar uncertainty is introduced by our calculation of hard X-ray flux (or upper limit) which was done by convolution of the *INTEGRAL* image in hard band with the same spatial model as observed in the *ROSAT* band.

Nevertheless all these uncertainties do not change the conclusion that it is very unlikely that IC emission in the 44–107 keV band can reach flux levels comparable to the ISGRI/*INTEGRAL* sensitivity, unless the magnetic field is as low as $\text{few} \times 0.1 \mu\text{G}$. A possible spectral aging of electrons do not affect this conclusion. Indeed as is clear from Fig.7 for $B < 10 \mu\text{G}$ the Lorentz factor of ‘radio’ electrons is smaller for the electrons responsible for the IC emission at 75 keV. Therefore the life time is shorter for electrons emitting in radio and IC part of the spectrum has to be a power law (since a power law in radio is observed). In the opposite limit of fields stronger than $10 \mu\text{G}$ the expected IC flux is orders of magnitude less than *INTEGRAL* values even without account for any possible electron aging.

5. SUMMARY

The summary of main results from the deep observations of the *Coma* cluster with *INTEGRAL* and combining these observations with results of *RXTE* and *ROSAT* observatories lead us to the following conclusions:

- 1) The total cluster spectrum in the 0.5–50 keV energy band is well described by the thermal plasma emission with the mean temperature $T \simeq 8.2$ keV;
- 2) There are significant temperature variations within the cluster and the mean 8.2 keV temperature is the result of mixing emission components with T ranging from 7.5 to 10.5 keV. The temperature near the *ROSAT* surface brightness peak is ~ 8.5 keV.
- 3) We do not detect a significant excess over the thermal spectrum at high energies. The upper limit on the non-thermal flux is, however, consistent with the previous detections reported on the basis of *Beppo-SAX* and *RXTE* observations.
- 4) It is very unlikely that IC emission in hard X-rays can reach the flux level comparable with the *INTEGRAL*/ISGRI sensitivity for the magnetic fields of $\text{few} \times 0.1 \mu\text{G}$.

This work is based on observations with *INTEGRAL*, and made use of the *INTEGRAL* Science Data Center (Versoix, Switzerland), Russian Science Data Center of *INTEGRAL* (Moscow, Russia) and the High Energy Astrophysics Science Archive Research Center Online Service, provided by the NASA/Goddard Space Flight Center. The work was supported by the *Chandra* grant GO5-6121A, RFBR grant 07-02-01051, DFG grant CH389/3-2, the “Extended objects in the Universe” program of the Russian Academy of Sciences, and a program of support for leading scientific schools (Project NSH-1100.2006.2). AL thanks CfA for hospitality during the course of this research.

REFERENCES

- Arnaud M., Aghanim N., Gastaud R., et al., 2001, *A&A*, 365, L67
 Briel U., Henry J. & Boehringer H., 1992, *A&A*, 259, L31
 Colafrancesco S., Marchegiani P. & Perola G., 2005, *A&A*, 443, 1
 Deiss B., Reich W., Lesch H., Wielebinski R., 1997, *A&A*, 321, 55
 Dogiel V., Colafrancesco S., Ko C., et al., 2007, *A&A*, 461, 433
 Dolag K., Bartelmann M. & Lesch H., 2002, *A&A*, 387, 383
 Eckert D., Neronov A., Courvoisier T., Produit N., 2007, *A&A*, 470, 835
 Ferrari C., Govoni F., Schindler S., et al., 2008, *Space Sci. Rev.*(accepted), arXiv:0801.0985
 Felten J. & Morrison P., 1966, *ApJ*, 146, 686
 Fusco-Femiano R., dal Fiume D., Feretti L., et al., 1999, *ApJ*, 513, L21
 Fusco-Femiano R., Orlandini M., Brunetti G., et al., 2004, *ApJ*, 602, L73
 Ginzburg V. L. & Syrovatskii S. I., 1965, *ARA&A*, 3, 297
 Jahoda K., Markwardt C., Radeva B., et al. 2006, *ApJS*, 163, 401

- Kim K.-T., Kronberg P., Dewdney P., Landecker T., 1990, ApJ, 355, 29
Krivonos R., Vikhlinin A., Churazov E. et al., 2005, ApJ, 625, 89
Krivonos R., Revnivtsev M., Lutovinov A., et al., 2007, A&A, 475, 775
Lebrun F., Leray J., Lavocat P., et al., 2003, A&A, 411,
Neuman , et al., 2003,
Renaud M., Belanger G., Paul J., et al., 2006, A&A, 453, L5
Rephaeli Y., 1979, ApJ, 227, 364
Rephaeli Y., Gruber D. & Blanco P., 1999, ApJ, 511, L21
Rephaeli Y. & Gruber D., 2002, ApJ, 579, 587
Rephaeli, Y., Nevalainen, J., Ohashi, T., & Bykov, A. M. 2008, Space Science
Reviews, 16 (arXiv:0801.0982)
Revnivtsev M., Gilfanov M., Sunyaev R., et al., 2003, A&A, 411, 329
Rossetti M. & Molendi S., 2004, A&A, 414, L41
Schlickeiser R., Sievers A. & Thiemann H., 1987, A&A, 182, 21
Snowden S., McCammon D., Burrows D., Mendenhall J., 1994, ApJ, 424,
714
Thierbach M., Klein U., Wielebinski R., 2003, A&A, 397, 53
Toor A. & Seward F., 1994, AJ, 79, 995
Tsygankov S., Lutovinov A., Churazov E., Sunyaev R., 2006, MNRAS, 371,
19
Tucker W., Kellogg E., Gursky H., et al., 1973, ApJ, 180, 715
Ubertini P., Lebrun F., Di Cocco, et al. 2003, A&A, 411, L131
Vikhlinin A., Forman W. & Jones C., 1997, ApJ, 474, L7
Vikhlinin A., Forman W. & Jones C., 1999, ApJ, 525, 47
Winkler C., Courvoisier T., Di Cocco G., et al., 2003, A&A, 411, L1